Cement and Concrete Research 40 (2010) 831–844

Contents lists available at ScienceDirect

Cement and Concrete Research

journal homepage: http://ees.elsevier.com/CEMCON/default.asp

Dissolution theory applied to the induction period in alite hydration

Patrick Juilland [a,*], Emmanuel Gallucci [a], Robert Flatt [b], Karen Scrivener [a]

[a] EPFL-STI-IMX– Laboratoires des Matériaux de Construction, Station 12, CH-1015 Lausanne, Switzerland
[b] Sika Technology A.G., Corporate Research and Analytics, CH-8048 Zürich, Switzerland

ARTICLE INFO

Article history:
Received 23 July 2009
Accepted 14 January 2010

Keywords:
Alite
Hydration (A)
Dissolution (A)
Induction period
Ca_3SiO_5 (D)

ABSTRACT

The early hydration of alite, in particular the reason for the onset of the induction period, has been a subject of controversy for many decades. Several theories have been proposed, principally the formation of a protective phase inhibiting dissolution or delayed nucleation and growth, but none have successfully taken into account all the experimental data available. This paper proposes a new mechanism, based on a geochemical approach to crystal dissolution that fully explains the origin of the induction period. It implies that during cement hydration, dissolution is initially dominated by the formation of etch pits on surfaces and later becomes limited to step retreat from such pits. This change in mechanism alone can account for the rapid decrease in reaction after first contact with water, without the need to invoke the formation of a protective phase. Furthermore it can explain all the experimental findings in the literature. While this geochemical view of dissolution explains many features of the induction period it does not account for its end. This remains a question for further research, but the most probable explanation appears to be the onset of rapid growth of C–S–H.

1. Introduction

The dissolution kinetics of minerals is a topic of broad concern in areas as diverse as: geochemistry [1–3], chemical engineering (reacting time; scaling deposits; etc) [4,5], construction materials (concrete, repair mortars, gypsum wall boards, etc.) [6–9], conservation of cultural heritage (stone dissolution by acid rain) [10–12], bioengineering (hydroxyapatite bone replacement cements) [13], storage of hazardous materials [14]. In recent years, significant work has been carried out on this topic, pioneered by Lasaga and Lüttge [2] in the area of geochemistry. In particular, they have shown that the mechanism of dissolution changes in nature as the solution concentration passes a critical undersaturation. In the paper we show that these findings have profound implications for understanding of the hydration of Portland cement, the binder in concrete which is the most used material in the world.

Portland cement is a low cost material with comparatively low environmental impact and can be produced from readily available local materials almost anywhere in the world. Nevertheless, the huge volumes consumed mean that overall cement production accounts for 5–8% of man-made CO_2 emissions. In order to improve sustainability it is very important to understand the basic mechanisms of hydration which is the process by which cement powder plus water transform from a fluid suspension to a porous solid over a matter of hours and strength develops over days and months. Tricalcium silicate, containing minor impurities such as alumina or magnesium oxide (alite), is the principal phase in Portland cement. On reaction with water it forms a calcium silicate hydrate phase of variable composition, C–S–H, and crystalline calcium hydroxide referred to as portlandite, CH [15]. Several major reviews on the mechanisms of hydration have been published [15–18]. Even though the phase transformations during the first 24 h are well documented, reactions at very early ages are still a subject of controversy, particularly regarding the so called induction or "dormant" period where the rate of reaction slows down dramatically after a short burst of rapid reaction on contact with water. It is often stated in the literature that the hydration of cementitious materials is a dissolution–precipitation process as originally proposed by Le Châtelier [19], but very few publications have given much consideration to the role of alite dissolution [6–9], in determining hydration kinetics.

In this paper we discuss the different theories on the early hydration of cementitious materials in relation to concepts of crystal dissolution established in the field of geochemistry.

New experimental results are then presented, which indicate that the slowdown in reaction can be explained by the dominant role of the dissolution process, governed by the saturation state of the solution as well as the density of crystallographic defects.

2. Theories of early hydration

Fig. 1 presents the heat flow monitored by isothermal calorimetry as well as the evolution of the calcium concentration during the early

* Correspondence author. Tel.: +41 21 693 68 59; fax: +41 21 693 58 00.
E-mail address: patrick.juilland@epfl.ch (P. Juilland).

0008-8846/$ – see front matter © 2010 Published by Elsevier Ltd.
doi:10.1016/j.cemconres.2010.01.012

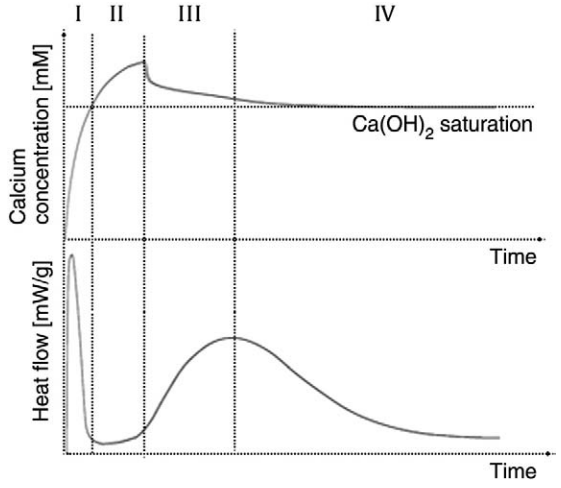

Fig. 1. Schematic representation of the different periods during the hydration of alite. Period I represents the rapid dissolution of the anhydrous phase, period II is a period of low chemical activity called the induction period, period III is the acceleration period in which massive precipitation of hydrates (C–S–H and CH) occurs and finally period IV is the deceleration period where the rate of hydration decreases gradually. Adapted from [15].

hydration of alite. The hydration of alite is generally divided in several time periods depending on the changes in rate of reaction during each time period. In this paper we are concerned with periods I and II. Period I is generally referred to as the initial dissolution period in which the rate of reaction rapidly slows, leading to period II in which the rate of reaction is low – generally known as the induction period. Without the presence of retarding admixtures, a distinct induction period – i.e. prolonged period of low heat output, may not be clearly identifiable. Nevertheless the initial slowdown in reaction after the addition of water, and the time before onset of the acceleration period still need to be explained. Many theories, summarised in Table 1, have been proposed to explain these phenomena.

2.1. Protective phase

One of the earliest, and still most widely accepted, theories for the first deceleration period is the formation of a protective layer of hydration products on the surface of the reacting grains which limits the dissolution of the anhydrous phase. Stein and Stevels [20] postulated that "a hydrate is formed fitting closely the C_3S surface". Hydration is claimed to reinitiate when this hydrated layer is removed or "converted" and the anhydrous surface again comes into contact with water. For example, Kantro and co-workers [21] and Stein and Stevels [20] proposed that the primary hydrate converts into another one less closely fitting the anhydrous surface and more permeable to water. It has also been proposed that the rupture of a protective membrane is caused by an osmotic pressure [28,29], but little experimental evidence has been found to support this theory.

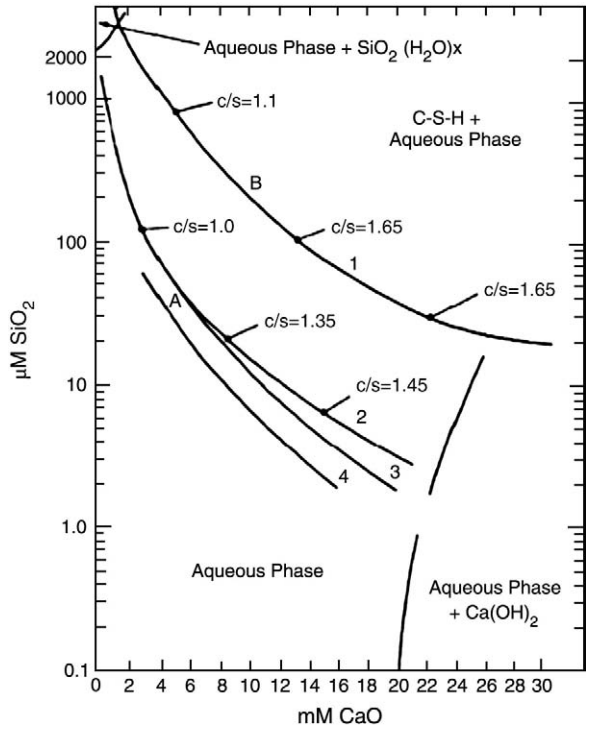

Fig. 2. Water-rich region of the $CaO–SiO_2–H_2O$ phase diagram showing the solubility curves of two types of C–S–H. Curve A represents three possible solubilities for C–S–H formed from soluble salts. Curve B represents the solubility of a C–S–H formed from hydrating C_3S or by precipitation from solutions of $Ca(OH)_2$ and silicic acid; from [22].

The study by Gartner and Jennings [22] on solution concentrations provides some of the strongest evidence for the existence of an impermeable hydrate. They identified two distinct trends in the data (Fig. 2), which they claimed indicate the existence of two forms of C–S–H, one with higher solubility (SI) being metastable with respect to the other (SII). They postulated that "the first-formed C–S–H (SI) has protective characteristics responsible for the period of slow reaction and that a solid-state transformation to a less protective form of C–S–H (SII) occurs at a molar ratio of CaO to SiO_2, around 1.7". However, it has never been possible to observe experimentally such a protective layer. In the corrosion of metals, where such protective layers are formed there is always an epitaxial relationship between the reacting metal and the protecting oxide. It is difficult to envisage such a relationship for such different crystal structures as C_3S and C–S–H. Gartner and Gaidis [23]

Table 1
Causes of the induction period and its termination [15–18].

Causes	Description	References
Protective membrane	The product of the initial reaction forms a protective layer on the C_3S particles; the induction period ends when this layer is destroyed or rendered more permeable by ageing or phase transformation.	[20–27].
Semi-permeable membrane	The product of the initial reaction forms a semi-permeable membrane which encloses an inner solution and is destroyed by osmotic pressure.	[28,29].
Double layer theory	The ions released in solution during the initial reaction inhibit further dissolution of the C_3S particles by lowering locally the undersaturation. The induction period ends when supersaturation with respect to hydrates is achieved and massive nucleation and growth occur.	[18,30].
Crystallographic defects	The length of the induction period is related to the density of crystallographic defects. The induction period ends when supersaturation with respect to hydrates is achieved and massive nucleation and growth occur.	[31–34].
Nucleation of CH	The induction period occurs because CH nuclei are poisoned by silicates and cannot grow. The induction period ends when the level of supersaturation is sufficient to overcome this effect.	[30,41].
Nucleation of C–S–H	The rate of reaction in the induction period is controlled by nucleation and growth of the C–S–H formed initially; the induction period ends when growth begins.	[6,34–36].

proposed that the slowdown in reaction rate is controlled by the formation of a layer of metastable C–S–H on the dissolving C_3S surface. Its thickness is unlikely to be uniform and is expected to be greater around the reactive sites. This metastable hydrate would then be consumed progressively by the precipitation of a more stable form of C–S–H that would lead to a more rapid dissolution providing a feedback mechanism. This feedback mechanism would allow the dissolution rate of the anhydrous phase to closely follow the C–S–H growth rate during the acceleration period.

Further evidence cited in support of the existence of a protective product comes from the study of Rodgers et al. [37] of tricalcium silicate hydration with cross-polarisation NMR. This indicated that monomeric hydrated silicates are formed at early ages of hydration and that hydrated silicate dimers are detected only from the end of the induction period. From the quantity of hydrated monomers it was calculated that if these belonged to an even layer on the surface, its average thickness would be around 40 nm. However, NMR does not provide any information on the spatial distribution of these hydrates, which may be very heterogeneously distributed. Furthermore, the same type of measurements on systems with additions of calcium chloride (an accelerator) and sucrose (a retarder) indicated that; in the case of calcium chloride, the formation of this monomeric species was much more rapid and a greater amount formed, but the induction period was shorter; whereas in the case of sucrose, the formation of the monomeric species was much lower but resulted in a very long induction period. Therefore it appears that the rate of formation and amount of these primary hydrates are poorly related with the "protective" properties of the product.

2.2. Double layer theory

An alternative theory to that of a protective layer invokes the formation of an electrical double layer with a build up of calcium ions close to the surface which inhibits further dissolution [18]. Tadros et al. [30] proposed that the formation of a double layer requires incongruent dissolution to give a charged SiO_2-rich surface layer, but surfaces, by their very nature involve unsatisfied bonds and therefore surface charges so this step of incongruent dissolution is not necessary according to this theory, the acceleration period is triggered by the precipitation of phases that consume calcium ions from solution which leads to a gradual breakdown of the double layer [17]. Such a mechanism is well recognised in other domains related to surface–solution interfaces (see [3,38–40]).

2.3. Nucleation and growth

Other theories postulate that the length of the induction period is governed by the nucleation and growth of hydrates — either CH or C–S–H [6,34–36]. Theories claiming that the nucleation of CH is rate determining suggest that this hydrate is not precipitated, even after the saturation of the solution with respect to this phase, due to a poisoning of the nuclei by silicate ions [30]. When the supersaturation of the solution with respect to CH becomes high enough to overcome the poisoning effect of adsorbed silicate ions, CH starts to precipitate. Young and co-workers [41] confirmed by analysis of the liquid phase composition that the induction period ends when the calcium concentration in solution reaches a maximum. At this point the calcium ion concentration is around 1.5 to 2 times the concentration of a saturated solution of CH in water [24]. However, the precipitation of CH and the consequent decrease in calcium concentration at the end of the induction period could be just a consequence (rather than the cause) of the onset of rapid hydration. Experiments on addition of CH to hydrating C_3S were shown to prolong the induction period, which was taken as evidence against CH precipitation being the rate determining process [15]. Furthermore, in dilute solutions the rapid onset of C–S–H formation occurs significantly before CH precipitation [42]. These observations indicate that the role of CH precipitation is not trivial and still needs clarification.

Others have argued that the rate of reaction during both the induction and the acceleration period is controlled by nucleation and growth of C–S–H nuclei [35,36,43]. From this point of view, the induction period ends when growth of C–S–H nuclei starts. However, there is substantial evidence that C–S–H precipitates minutes, if not seconds, after the addition of water [44,45]. Garrault et al. [36,43], claim that nuclei form at the very beginning of the hydration reaction and argue that there is no true induction period but a continual increase in the rate of C–S–H formation. However, most of their studies relate to hydration in dilute suspensions saturated with respect to lime, as discussed later the mechanisms operating in this case may differ significantly from those in pastes at more practical water to cement ratios.

All theories where nucleation is the rate determining factor for the end of the induction period fail to address the question of the rapid slowdown of the reaction in the first few minutes.

3. Dissolution of crystals: concepts from geochemistry on the role of crystallographic defects and solution saturation

Dove and co-workers showed that mechanisms analogous to those used in classic crystal growth theory can explain the dissolution behaviour of many minerals (quartz, feldspar, olivine, gibbsite, calcite, etc.) and even protein crystals [1,46,47]. Dissolution can be simply described as the inverse of nucleation and growth, as suggested by Cabrera and Levine [48] for calcite in 1956. There are three main mechanisms of dissolution presented in Fig. 3: formation of 2D vacancy islands, etch pit formation at dislocations and step retreat at pre-existing roughnesses. The first two have defined activation energies, ΔG^n_{crit} and ΔG_{crit} ($\Delta G^n_{crit} \geq \Delta G_{crit}$).

The energy to overcome these activation energy barriers is provided by the undersaturation, σ, of the solution (NB the undersaturation σ is also referred to as ln(SI) in some publications).

$$\sigma = \frac{\Delta\mu}{kT} = \frac{\Delta G^*}{RT} = \ln\left(\frac{Q}{K_{SP}}\right) = \ln(SI) \quad (1)$$

where σ is the undersaturation coefficient, ΔG^* the free energy difference between the solution and the solid phase for dissolution

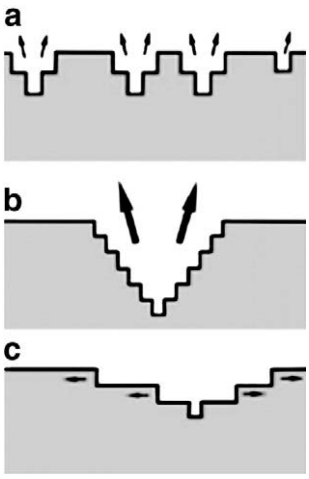

Fig. 3. Dissolution mechanisms: (a) two-dimensional vacancy islands: nucleation of small pits at perfect surfaces with or without the help of impurities; (b) etch pit: formation at the outcrops of a dislocation with the surface; and (c) step retreat taking place at pre-existing roughness. Mechanisms (a) and (b) are fast dissolution processes occurring at far from equilibrium conditions. (c) is a slow dissolution mechanism occurring at close to equilibrium conditions.

into solution of activity product Q, $\Delta\mu$ the difference in chemical potential, k the Boltzmann constant, R the gas constant, T the temperature, Q the ratio of the activity products to reactant species raised to the power of their stoichiometric coefficient, K_{SP} the mineral solubility product, and SI is defined as the saturation index [1–3]. Note that SI<1 for undersaturated solutions which means that σ, $\Delta\mu$ and ΔG^* are negative values.

Depending on the undersaturation, three regimes of dissolution are delimited by two activation energies. For very large undersaturations two-dimensional pits can nucleate on surfaces without the presence of dislocations (Figs. 3(a) and 5, mechanisms (a) and (a′)) [49]. However, as with the homogeneous nucleation of precipitates, the activation energy for this mechanism is high, so this regime is not expected to operate much in cementitious systems, apart possibly for very short time and when using ultrapure water.

Dove and co-workers [1] have established a general expression for the free energy barrier for nucleation of a two-dimensional pit on a surface, ΔG^n_{crit}:

$$\Delta G^n_{crit} = -\frac{\pi\gamma^2\Omega h}{N_A\Delta\mu} = -\frac{\pi\gamma^2\Omega h}{\Delta G^*} \quad (2)$$

where h is the step height, γ the solid–liquid interfacial energy, Ω the molar volume, N_A the Avogadro number, $\Delta\mu$ and ΔG^* are the same parameter defined in Eq. (1).

The interfacial energy may be modified by the presence of defects or impurities, which can decrease it significantly compared to the surface free energy of a perfect crystal.

As the undersaturation decreases, the activation barrier ΔG^n_{crit} increases and it is eventually no longer possible to nucleate etch pits on plain surfaces. On the other hand, etch pits can continue to form where dislocations intersect the surface. The second free energy barrier concerns this process ΔG_{crit} and is defined by:

$$\Delta G_{crit} = \Delta G^n_{crit}\cdot\sqrt{1-\xi} \quad (3)$$

with ξ is defined as:

$$\xi = \frac{N_A S b^2 \alpha}{2\pi^2\gamma^2\Omega}\cdot\Delta\mu \quad (4)$$

where γ is the solid–liquid interfacial energy, Ω the molar volume in the crystal, N_A the Avogadro number, S is the shear modulus, $\mathbf{b}$ the Burgers vector of the dislocation, and $\alpha = 1/(1-\nu)$ for a clean edge dislocation and $\alpha = 1$ for a clean screw dislocation (where ν is Poisson's ratio): $\Delta G_{crit}\to 0$ when $\Delta\mu\to -\frac{2\pi^2\gamma^2\Omega}{N_A S b^2\alpha}$, which therefore defines the critical undersaturation above which etch pit formation is spontaneous at dislocations:

$$\sigma_{crit} = \frac{\Delta\mu_{crit}}{kT} = \frac{\Delta G^*_{crit}}{RT} = \ln\left(\frac{Q_{crit}}{K_{SP}}\right) = -\frac{2\pi^2\gamma^2\Omega}{RTSb^2\alpha}. \quad (5)$$

(Complete details about these calculations can be found in [3]).

When the ionic activity is high and the undersaturation becomes lower than σ_{crit}, the formation of etch pits at dislocations is no longer spontaneous. The formation of new etch pits at dislocations rapidly stops and there is then a transition to a slow dissolution process controlled by step retreat at pre-existing steps (Figs. 3(c) and 5, mechanism (c)). The density of steps, and therefore rate of dissolution in this regime, will depend on the number of etch pits created previously. It should be noted that step retreat takes place regardless of the undersaturation, but since its rate is slow, its contribution to the overall dissolution rate is small at larger undersaturations.

Fig. 4 shows how these two energy barriers vary as a function of the undersaturation and indicates the delimitation of the three dissolution regimes for the case of albite. The value of surface energy and Burgers vector are those used by Burch et al. [50]. It is noted that their estimate of the surface energy of albite of 0.5 J/m^2, seems relatively high for a liquid–solid interface, considering solid–vapour surface energies are in the range 1–2 J/m^2. Nevertheless, this combination of values does

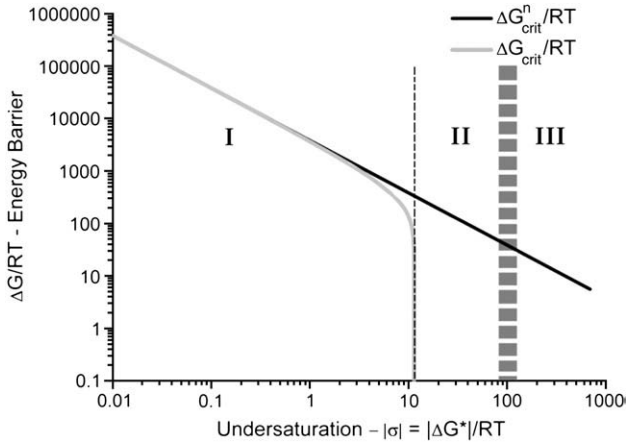

Fig. 4. Dependence of the two activation energy barriers $\Delta G_{crit}{}^n$ (2D vacancy islands) and ΔG_{crit} (etch pit) as a function of the undersaturation for an albite crystal at 80 °C having $\gamma = 0.5$ Jm^{-2}, $\Omega = 100$ cm^3/mol, $||\mathbf{b}|| = 7$ Å and G = 30 GPa. Values from [50]. In regimes I, II and III, step retreat, etch pit formation at dislocations and the formation of 2D vacancy islands are respectively the rate determining mechanisms. The transition between the second and the third regime is not as clearly defined as for the transition between the first and the second regime, it therefore why this transition is delimited by a broader separation.

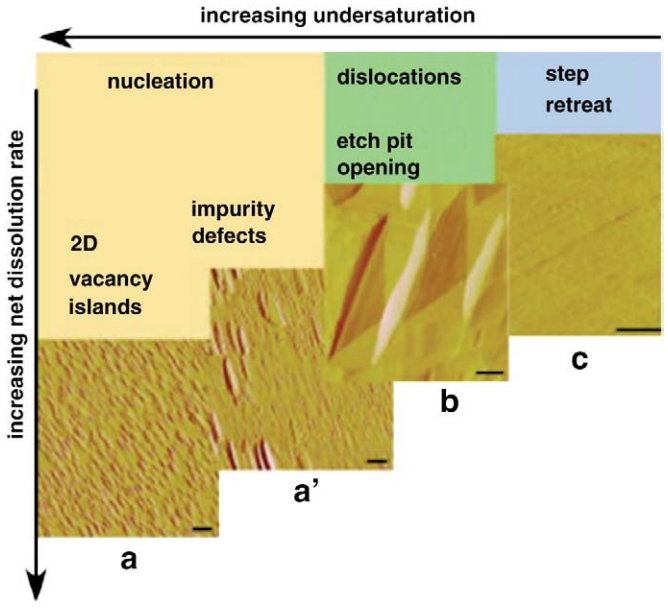

Fig. 5. AFM images of quartz (100) surfaces produced by dissolution in solutions of different chemistries after equivalent amounts of dissolution. (a) When $S = 0.10$ and the solution contains 0.0167 M $CaCl_2$, the surface is covered with a high density of small pits with flat bottoms and steep flanks. (a′) At an intermediate driving force of $S = 0.65$ in a salt solution of 0.0167 M $CaCl_2$, a mixture of larger and shallower flat bottom pits form across the surface. (b) When $S = 0.10$ in H_2O, surface are dominated by large etch pits with sloping sides that converge at dislocation sources. Pits are separated by relatively flat regions on the surface. (c) At a low driving force of $S = 0.90$ in 0.0167 M $CaCl_2$, surfaces shows only straight edge steps with no evidence of pitting. The associated equations between the different processes are Eq. (2) for the transition 2D vacancy islands-impurity defects and dislocations-etch pit opening and Eq. (3) for the dislocations-etch pit opening and the step retreat process. Adapted from [46].

explain quantitatively the transition in dissolution modes seen in Fig. 6, as discussed later.

Owing to variations in the size of the Burgers vector **b** and in the solid–liquid interfacial energy, different crystal faces will behave differently during etch pit formation and the number of etch pits will vary according to the types and number of dislocations present [51].

The principal features discussed above are illustrated in Fig. 5 for surfaces of quartz (100) under different undersaturation conditions [46].

Experimental results for the net dissolution rate of various minerals as a function of undersaturation (adapted from [2]) are shown in Fig. 6. Note that the dissolution rates are defined as negative value as opposed to growth rates. It can be observed that there are two regimes of dissolution, corresponding to the regime in which the undersaturation of the solution is low enough ($\sigma \ll \Delta G^*_{crit}$) to allow the formation of etch pits at dislocations, followed by a sharp decrease in the rate of dissolution at undersaturations, still quite far from equilibrium, where only step retreat can occur. (The regime of homogeneous formation of etch pits is not observed in these plots). Most of these minerals show large values of ΔG^*_{crit} — from 2 to tens of kJ/mol. Therefore, slow dissolution rates are observed not only close to equilibrium, but also quite far from it. For example in the case of albite the slowdown in dissolution, due to the fact that etch pits may no longer form at dislocations occurs at an undersaturation of around 11 (~33 kJ/mol) (Figs. 4 and 6). Phenomenologically this drastic slowdown in dissolution rate is similar to what is seen for alite. This observation led us to carry out some new experiments and re-examine published data on the early stages of alite and C_3S reaction.

4. New experimental results and reassessment of previous studies

4.1. Morphological studies of early age hydration of cementitious materials

In order to investigate the relevance of the above theories to the early dissolution process of alite, studies were made on alite synthesised by the authors, quenched in air [52] and then fractured to give fresh surfaces. The theory of dissolution presented above indicates that the state of saturation of the solution should be of great importance. The samples were immersed in two different solutions: deionised water and saturated lime solution for 2 and 30 min. The water to cement ratio was in the range of 1000. The samples were not coated for examination in the SEM; the pictures (Fig. 7) were taken in the secondary electron mode at an accelerating voltage of 3 kV.

After only 2 min samples immersed in water show extensive surface pitting. There is also a marked difference in Fig. 7(a) between the crystal in the top right of the picture and the one in the bottom left. This is a consequence of the crystallographic orientation of the grains, which would have different interfacial energies, different dislocations densities and therefore different energy barriers for the nucleation of pits. It is also pertinent to note that the clear definition of these etch pits suggests that there is no hydrate layer covering the surface. Furthermore, these reactive sites of dissolution cover the surface fairly evenly, so the formation of a protective phase only at reactive sites unlikely. After 30 min of hydration (Fig. 7(c)) one can observe that the surface has been severely corroded with step heights reaching several hundreds of nanometers.

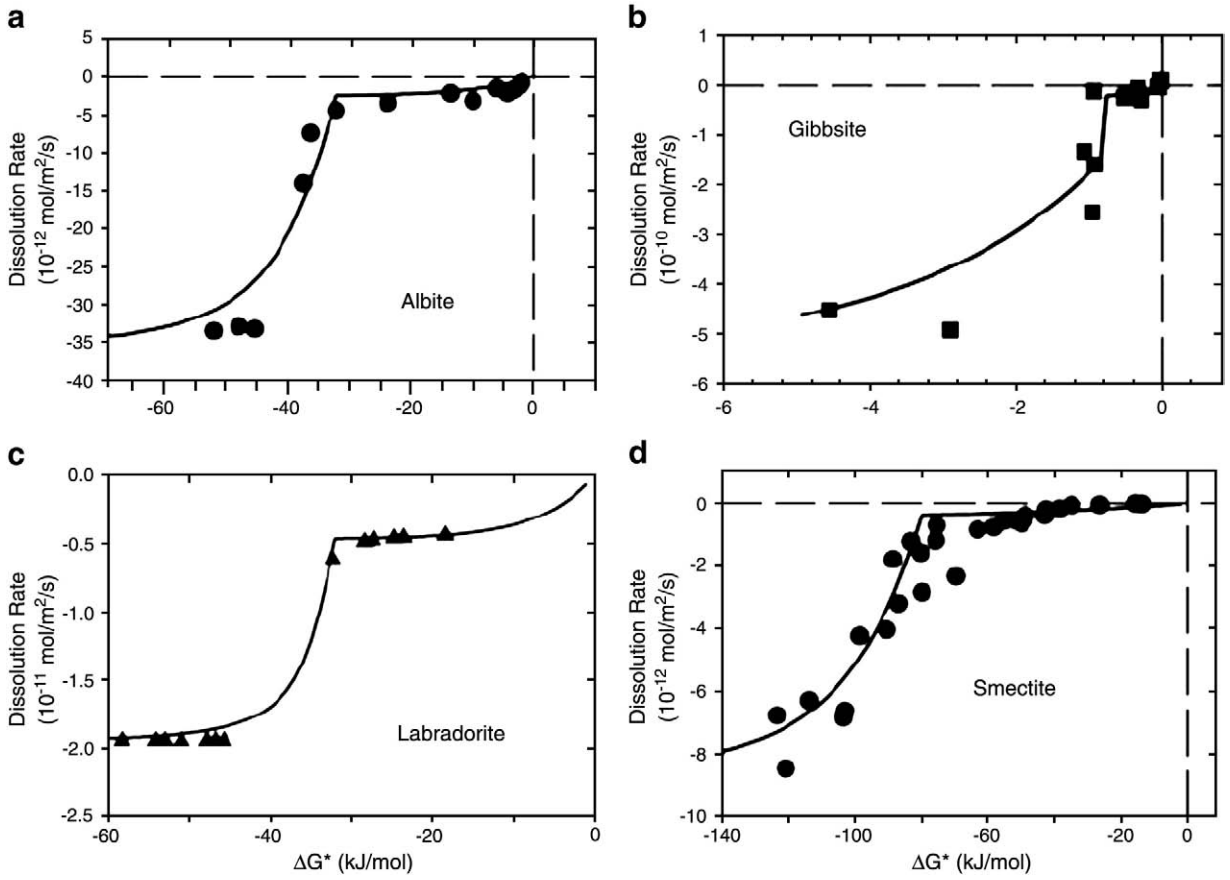

Fig. 6. Comparison of the full dissolution theory (see Eq. (5)) with experimental data of net dissolution rate. (a) Albite at pH 8.8 and 80 °C. (b) Gibbsite at pH 3 and 80 °C. (c) Labradorite at pH 3 and 25 °C. (d) Smectite at pH 3 and 80 °C. (Adapted from [2]).

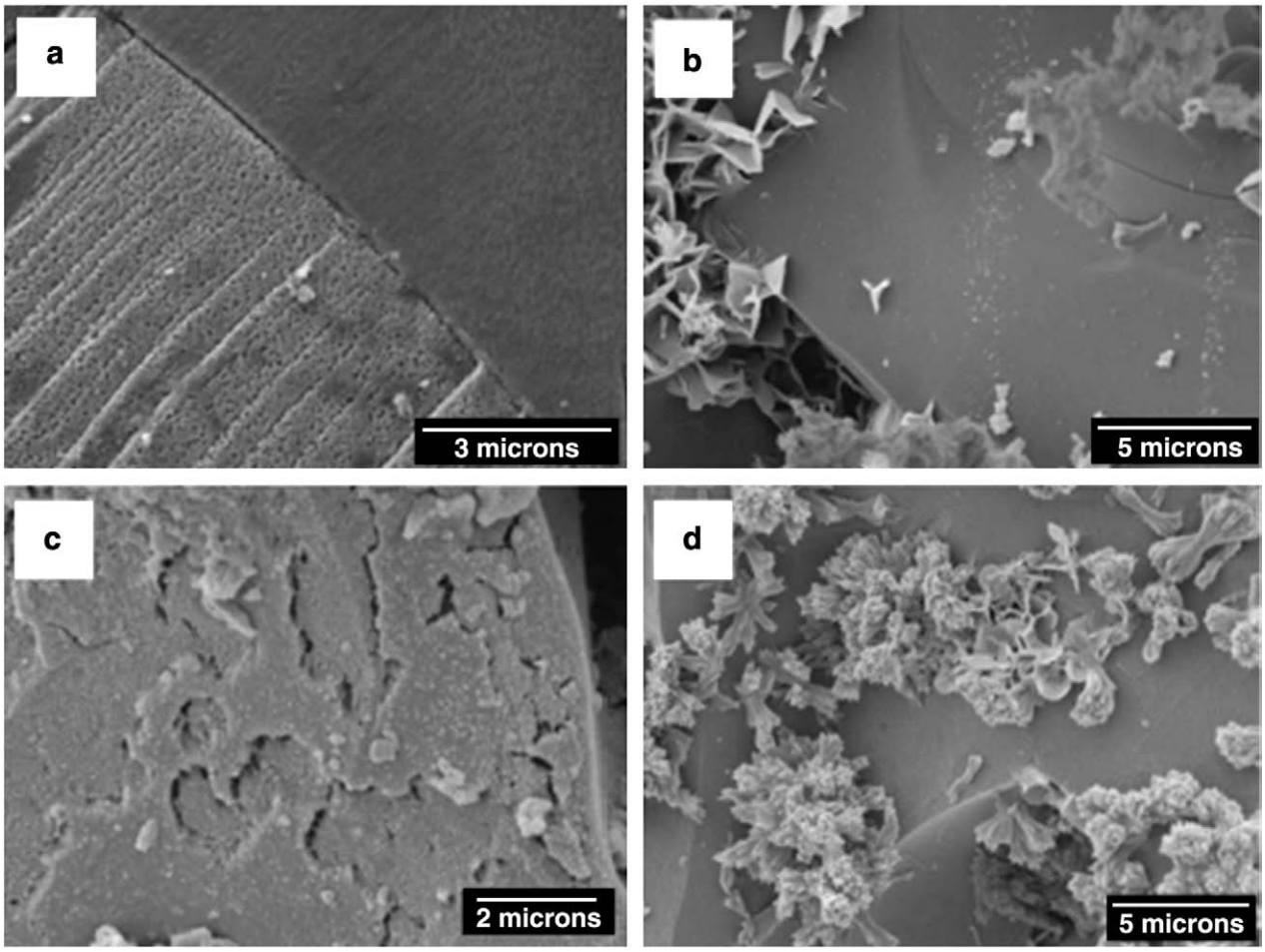

Fig. 7. SEM micrographs of alite immersed during 2 min in (a) deionised water, (b) saturated lime solution, and 30 min in (c) deionised water and (d) saturated lime solution.

In the case where the alite was hydrated in saturated lime solution, the surface does not undergo such extensive dissolution. After 2 min portlandite and other hydrates have precipitated, maybe during specimen drying or at places where supersaturation is locally reached (Fig. 7(b)). After 30 min (Fig. 7(d)), C–S–H with a "sheaf of wheat" morphology [53,54], is observed. However, at both times most of the surface appears smooth and unattacked. This strongly suggests that under saturated lime conditions, the predominant regime of dissolution is step retreat since the formation of etch pits is not observed for these samples.

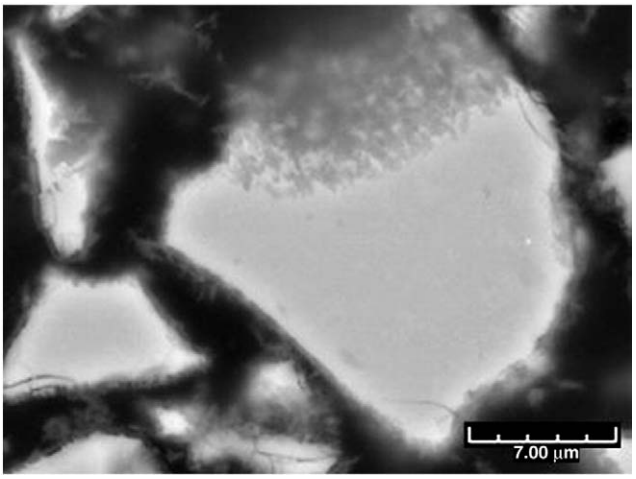

Fig. 8. Alite grain hydrated for 12 h in paste with a w/c = 0.5 [52].

These observations confirm that the concentration of the solution plays an important role in the dissolution process of alite as seen in studies of other minerals and explained in the previous section.

Fig. 8 from a normally hydrated alite paste shows that even at much later ages dissolution from certain areas is favoured to give a very rough surface, while other crystal facets show a much lower degree of reaction.

In fact, examination of the literature indicates other studies in which the effect of solution concentration on dissolution rate is apparent. For example, Barret and Ménétrier [6] analysed filtrates obtained by passing a limited amount of solvent (distilled water or lime solution at various lime concentrations) through C_3S spread on a millipore filter. They showed that the lime concentration increase was always smaller when the lime concentration in the solvent was high. Several studies on dilute suspensions with different lime concentrations in the aqueous phase have been undertaken during the past decades [36,42,55,56]. In Fig. 9, it can be seen that the first peak of dissolution monitored by isothermal calorimetry is completely different depending on whether the aqueous phase is pure water or a saturated lime solution. This clearly shows the effect of the initial saturation state of the early dissolution.

4.2. Induction period and crystallographic defects

In order to study the influence of crystallographic defects on the early reactions of alite with water, narrow particle size distributions of quenched alite were thermally-treated at 650 °C for 6 h. The particle size distributions were centred around values of d_{v50} of 38, 61 and 82 µm the particle size distribution is shown in (Fig. 10) [52].

The annealing temperature of 650 °C is one at which recovery – annealing of defects and a decrease in the number of dislocations – is

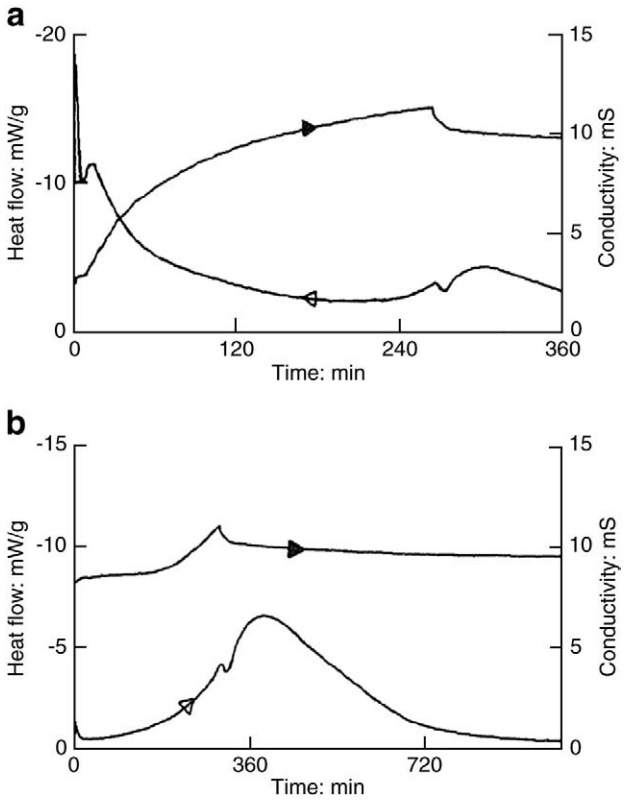

Fig. 9. Heat evolution and electrical conductivity curves plotted against hydration time for C_3S hydration (a) in water at a w/c = 18 and (b) in a 22 mM lime solution at w/c = 16, from [42].

expected to occur. The treated samples changed from polymorph MIII to TI as demonstrated by the X-ray diffraction patterns in Fig. 11, which is consistent with the decrease in defect density. The particle size distribution was however not affected by this heat treatment.

Narrow particle size distributions were chosen to avoid dispersion of the reactivity due to different particle sizes. The heat of hydration was followed by isothermal calorimetry at 20 °C, with a water to cement ratio of 0.4. Fig. 12 shows the heat evolution of the quenched and thermally-treated samples. Fig. 12(a), in which the samples were mixed inside the calorimeter, shows that the first heat peak is much smaller for the thermally-treated sample than for the control. In Fig. 12(b) the samples were mixed externally by hand before insertion into the calorimeter. The sharp initial heat peak is followed by a period of low chemical activity which is prolonged for several hours for the

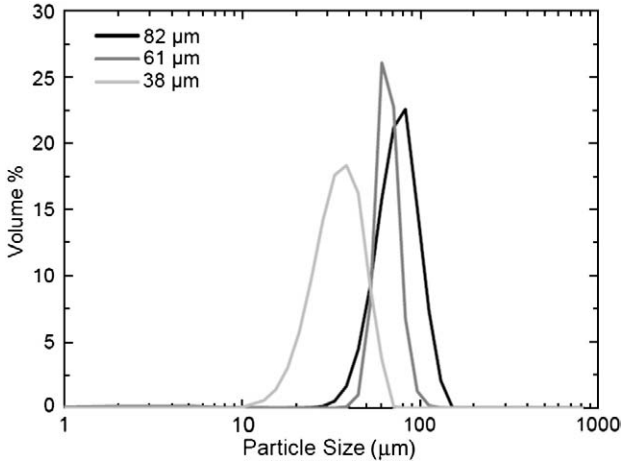

Fig. 10. Particle size distribution of alite used in this study [52].

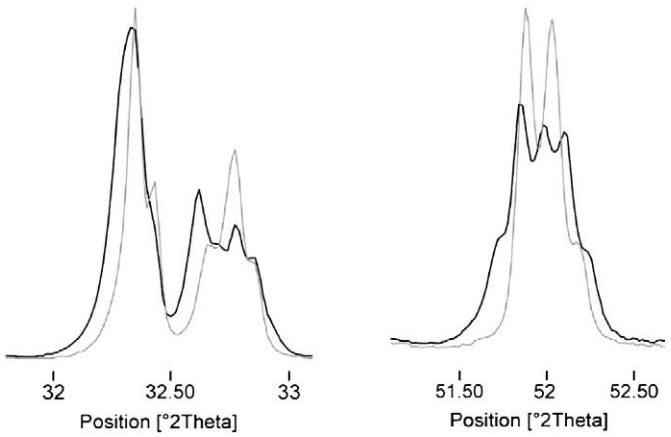

Fig. 11. Diffraction pattern of the reference alite in gray showing the MIII polymorph and the thermally-treated sample in black showing TI polymorph.

thermally-treated specimens, with a definite, almost flat, induction period. However, the acceleration and deceleration parts of the curves are very similar for both treated and untreated samples, which suggest that the same mechanisms and rate laws apply to both the quenched and the heat treated samples at this stage.

These experiments show that the early dissolution behaviour is dramatically affected by the defect density of the crystals and that this

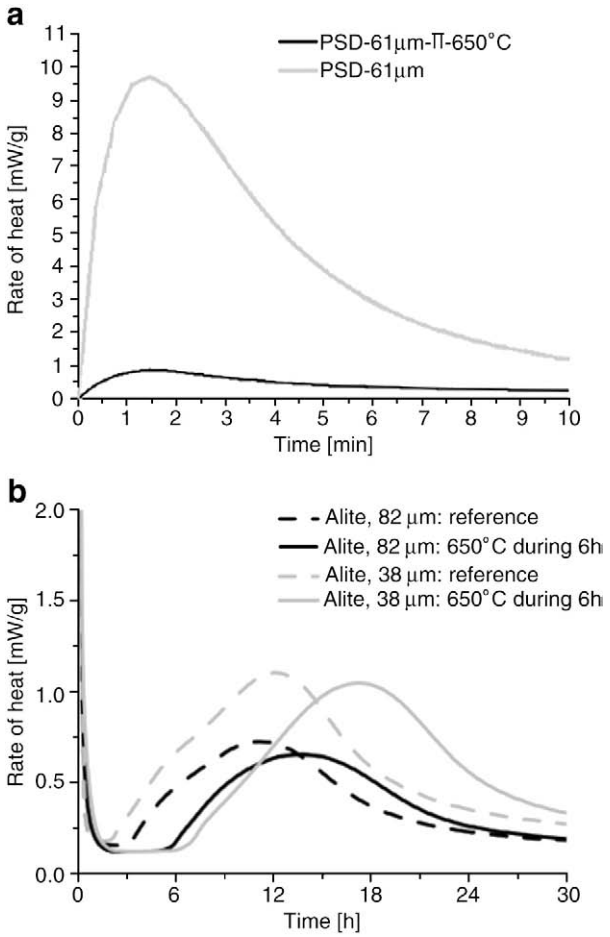

Fig. 12. Heat evolution of quenched alite (control) and alite thermally-treated at 650 °C for 6 h of narrow particle size (a) 61 µm during the first dissolution period (in-situ measurement) and, (b) 38 µm and 82 µm for the main peak of hydration. Dashed curves represent the thermally-treated samples. All measurements were performed at 20 °C and the water to cement ratio was kept at 0.4.

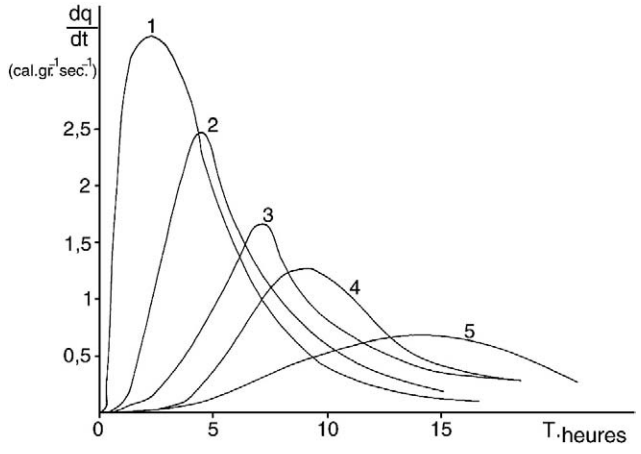

Fig. 13. Calorimetry curves of tricalcium silicate thermally-treated showing the effect of crystallographic defects on the length of the induction period resulting from different thermal treatments (curve 1 is the quenched alite whereas the other curves represent longer thermal treatment) [57].

affects the time needed to reach the acceleration period. According to the theory of dissolution, a low density of crystallographic defects will lead to a low number of etch pits. Therefore when dissolution becomes limited to the step retreat process (as the solution concentration increases) the surface is less rough due to the low number of etch pits so there are less steps. Therefore, dissolution proceeds at a lower rate compared to the quenched alite.

4.3. Previous evidence of the role of crystallographic defects on the reaction of cementitious materials

In fact, the role of defects in the early hydration processes of cementitious materials was already noted by previous researchers [31–34]. Maycock and co-workers [33] and Odler and Schüppstuhl [31] studied the effect of quenching rate on the reactions of alite and found that faster quenching, likely to induce more crystal defects, resulted in shorter induction periods. Fierens and Verhaegen [34] cooled tricalcium silicate at different rates from 1600 °C to 1300 °C before quenching. Besides calorimetry (Fig. 13), they used thermoluminescence to follow the changes during the early reaction [57,58]. Thermoluminescence gives an indication about the presence of crystallographic defects in the structure by excitation with plasma, γ ray, or UV sources followed by relaxation upon heating, leading to the emission of light [59]. Two populations of defects were identified, whose amount increased with higher cooling rates. One of these populations of defect progressively disappeared during early hydration. Furthermore, the length of the induction period was found to be inversely proportional to the original magnitude of this thermoluminescence peak. (The changes in the calorimetry curve are different to those reported above due to the fact that a broad range of particle sizes is present.).

Dislocations and planar defects (such as stacking faults) were observed by TEM in alite thermally-treated at (700 °C) by Hudson and Groves [60]. The density of dissociations in these annealed samples, was too low to be measured by TEM (the limit of resolution of TEM method for determining dislocation densities dislocation densities is around 10^6 cm^{-2} [61]). It is however not excessive to assume that surfaces of quenched alite should be intersected by numerous defects. Dislocations and stacking faults in alite would arise from the growth and cooling process, possibly affected by the presence of impurities, and during the grinding processes.

Sakurai and co-workers [32] etched alite with a solution of 0.4% HF with 0.6% HNO_3 in ethyl alcohol in order to reveal defects, grain boundaries, etc.

Their SEM images reproduced in Fig. 14 show that etching begins at grain boundaries and etch pits are formed that they associated with the emergence of dislocations.

Ménétrier and co-workers [45] observed by SEM a non-uniform attack of the C_3S surface exposed to water before growth of hydrates occurred (Fig. 15).

Etch pits have also been observed recently by Makar and Chan [62] for commercial Portland cements hydrating at a water to cement ratio of 0.5 (Fig. 16). All these examples showing the presence of etch pits on the surface of the grains tends to contradict the presence of a protective coating and especially the one covering reactive sites as proposed by Gartner and Gaidis. The fact that pits can be observed is a proof that no coatings are formed on these reactive sites and in the images from Makar and Chan hydration products can be seen in other places.

By atomic force microscopy, Garrault et al. [43] observed preferential dissolution, forming parallel steps, during the early hydration of a polished section of alite in saturated lime solution. This could correspond to a slow dissolution process by step retreat occurring at the low undersaturation provided by the saturated lime solution they used. Similar studies by di Murro [63] show the evolution of the surface in function of time, Fig. 17. These images were interpreted as showing nucleation and growth of C–S–H. However, re-examination of these images suggests that they in fact show surface dissolution with the formation of steps as arrowed in Fig. 17, (b). It can also be observed that dissolution of the surface does not occur evenly, demonstrating the importance of the crystallographic orientation. It should be noted that these AFM studies were carried out with liquid solution on the surface, confirming that the absence of protective hydrates in the SEM is not just an artefact of specimen preparation.

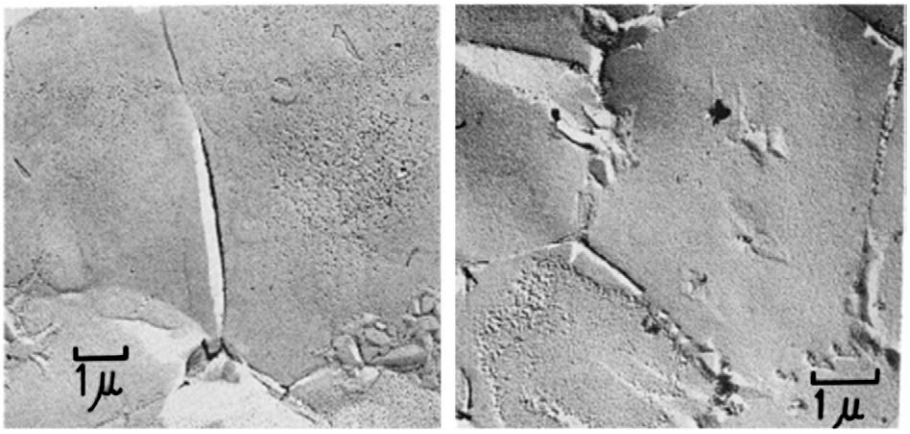

Fig. 14. SEM micrographs of C_3S samples with 1.1% wt. Cr_2O_3 after 1 min in etchant (0.4% HF with 0.6% HNO_3 in ethyl alcohol) [32].

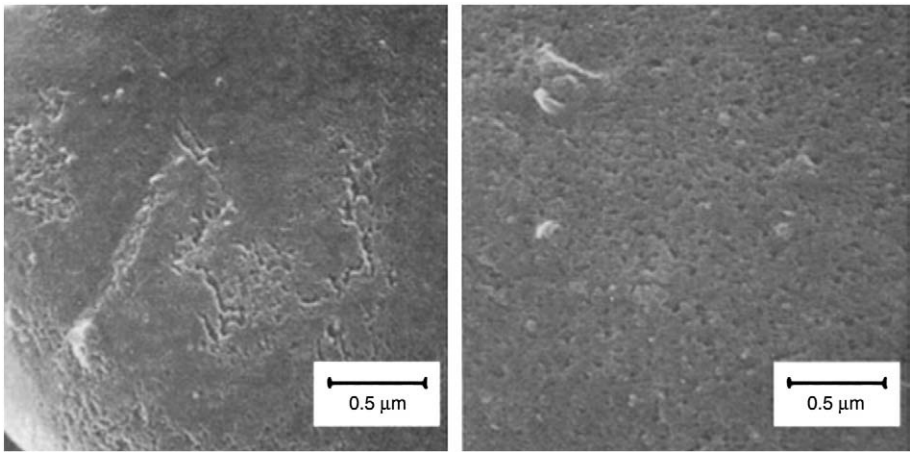

Fig. 15. High-resolution SEM micrographs of hydrated C_3S surface at w/c = 1.0 [45].

5. Discussion

5.1. Large difference from solubility limit of C_3S

One of the main objection to theories which do not invoke the formation of a protective layer is the difficulty to account for the large discrepancy between the calculated ion activity product of about 10^{-18} measured experimentally in solution (using calcium and silicate concentrations of 10–20 mM and 50–200 µM respectively at a pH 12) and the expected equilibrium value K_{SP} of around 3 [64]. Using this value in Eq. (1) would give an undersaturation coefficient of about −38 to −43 for saturated lime conditions, where it is already observed experimentally that etch pits do not form. This value is larger than the typical values of other minerals at the onset of slow dissolution of around 11 discussed earlier. Fig. 18, below, shows the variation in the dissolution regimes as a function of surface energy, compared to the data for albite shown in Fig. 4. An alite–water interfacial energy of around 1.06 J/m^2 would be needed for etch pit formation at defects to cease at undersaturations of below about 43. The surface energy of alite in water is not known and cannot be measured, due to the strong reaction. This value seems high compared to the estimated alite-vapour surface energy of 1.5 J/m^2 [65]. However, it is possible that there is not much relaxation of the alite surface, due to the initial fast reaction. Such surface relaxation will affect only the outer 1–2 atomic layers and cannot be equated with the formation of a separate phase, even if may lead to important changes in surface energy.

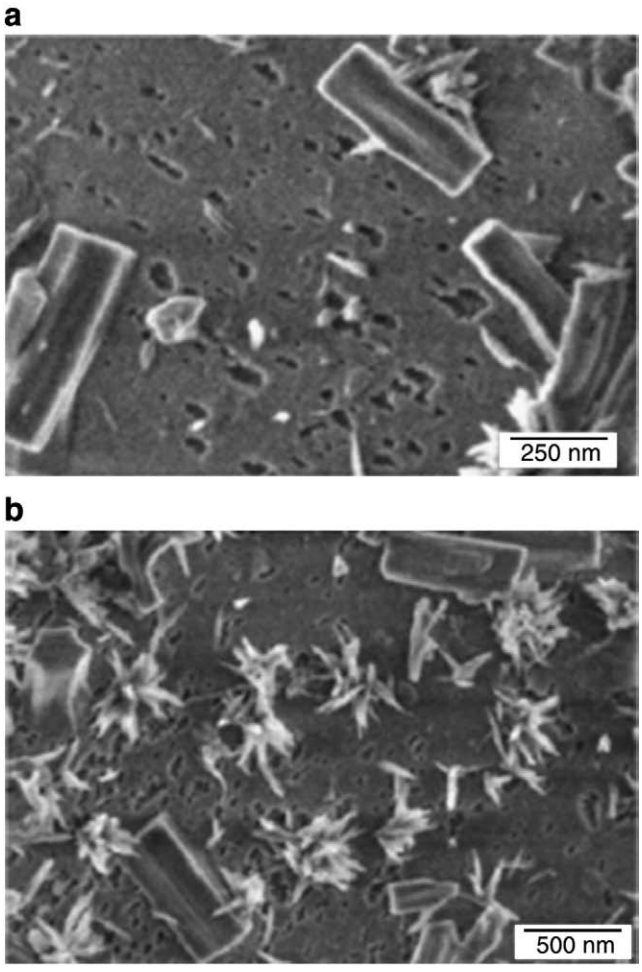

Fig. 16. Morphology of ordinary Portland cement at different times of hydration (w/c = 0.5). (a) After 180 min of hydration and (b) after 240 min, from [62].

5.2. Calculations of dissolution rate

Transition state theory (TST) is often used to predict the rates of reactions of mineral–fluid interactions [66]. TST predicts an exponential dependence of the reaction rate on $\Delta G_r^*/RT$, where ΔG_r^* is the Gibbs free energy of the overall reaction given by [50] (written for dissolution):

$$Rate = A\left[1 - e^{\frac{n\Delta G_r^*}{RT}}\right]. \quad (6)$$

Where A and n are general constants. This equation is derived from the original equation where n is equal to 1 which represents a single rate-limiting elementary reaction mechanism. It has been shown that TST cannot be used to predict rates near equilibrium conditions from those determined at high undersaturation conditions [50]. The reason for this is that TST is not able to catch the nonlinearity due to the transition between dislocation-controlled to step retreat dissolution mechanisms as illustrated for the case of albite in Fig. 19.

Fig. 19 shows the comparison of TST predictions (see Eq. (7)) with experimental data for albite, [50]. Eq. (6) is applied for the case of albite where the dissolution rate at high levels of undersaturation was determined as $-33.2 \cdot 10^{-12}$ mol/m^2/s. The dashed, dark gray and black lines in Fig. 19 correspond, respectively, to values of $n = 0.1$, 0.5 and 1.0. It can be seen that it is not possible with transition state theory to correctly model rates of dissolution when the solution is close to equilibrium conditions using parameters determined from far equilibrium conditions.

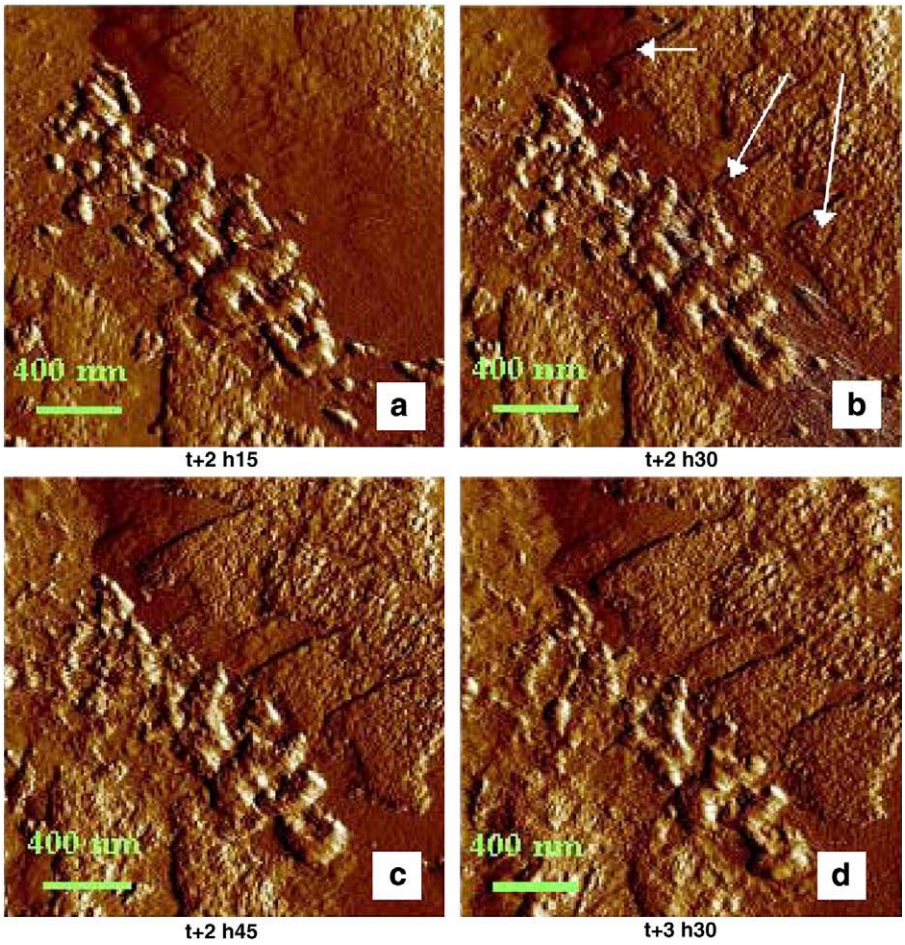

Fig. 17. Topographic observation by AFM of alite surface hydrating in a saturated lime solution (deflection mode). From images a–b–c–d, it is possible to observe the dissolution of specific crystallographic planes (white arrows in (b)). (AFM images from [63]).

It is worth noting that through Eq. (6), the TST predicts that the dissolution rate should reach a constant value at high undersaturation, which is indeed observed in Fig. 19. The major prediction of the TST, which is the variation of the rate between low and high undersaturation is however clearly unsatisfactory. This type of conclusion was also reached for C_3S by Bullard [67], who developed a kinetic cellular automaton model that includes transition state kinetics. He found that the data could however be fitted if a metastable C–S–H layer, of which the properties had to be obtained by fitting, was incorporated into the model [67]. More recently he reported that the same data could be almost equally well fitted if the C_3S surface is assumed to have a much lower solubility [68].

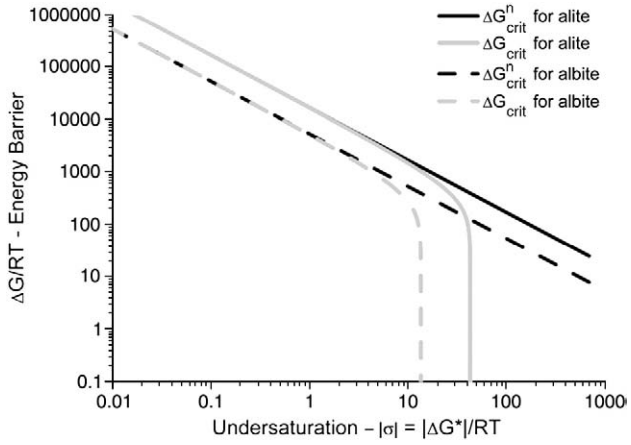

Fig. 18. Dependence of the activation energy barriers for the nucleation of 2D-vacancy islands (ΔG^n_{crit}) and etch pit formation (ΔG_{crit}) with different assumed solid–liquid interfacial energies; $\gamma = 500\ mJ\ m^{-2}$ for albite and $\gamma = 1060\ mJ\ m^{-2}$ for alite. The other parameters are kept the same as in Fig. 3 except for the molar volume, which is equal to $70\ cm^3\ mol^{-1}$ for alite. The intersection between the abscissa and the plain curves give the values of $|\Delta G_{crit}^*|/RT$ above which etch pits can form at dislocations.

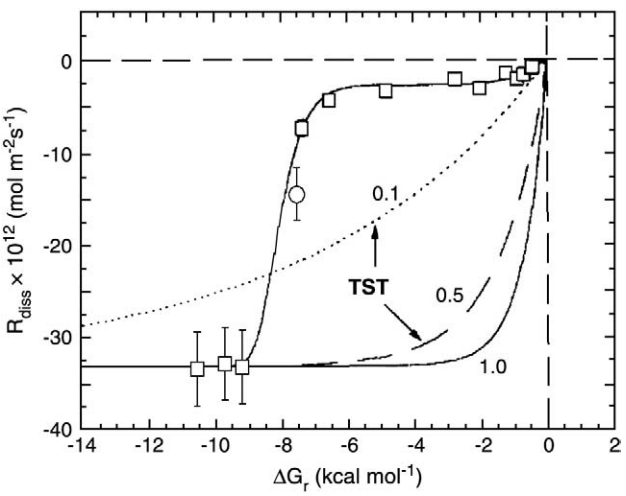

Fig. 19. Comparison of the full dissolution theory (see Eq. (5)) with experimental data and transition state theory. Albite at pH 8.8 and 80 °C. (From [50]). The dotted dashed, black lines correspond, respectively, to values of $n = 0.1$, 0.5 and 1.0 in Eq. (6).

However, there are other ways to overcome the limitation of TST and to fit experimental data on a large range of undersaturation conditions, Lasaga proposed this general equation for the rate of dissolution of mineral [66]:

$$Rate = k_0 \cdot A_{\min} \cdot e^{-E_a/RT} \cdot a_{H^+}^{nH^+} \cdot \prod_i a_i^{n_i} \cdot g(I) \cdot f(\Delta G_r) \quad (7)$$

where

- k_0 is the rate constant (average or instantaneous at $t=0$),
- $A_{\min}$ is the reactive surface area of the mineral,
- $e^{-E_a/RT}$ is a term related to the temperature dependence,
- $a_{H^+}^{nH^+} \cdot \prod_i a_i^{n_i}$ where a_i and a_{H^+} are the activities in solution of species i and H^+, respectively, n_i and nH^+ are the orders of the reaction with respect to these species. This represents a pH dependence of the dissolution reactions and other possible catalytic effects on the overall rate,
- $g(I)$ is a function of the ionic strength. The $g(I)$ term indicates a possible dependence of the rate on the ionic strength (I),
- $f(\Delta G_r)$ relates the velocity of the dissolving steps from a dislocation core as a function of the change in Gibbs free energy upon dissolution.

Damidot et al. [9] showed that the rate of dissolution of alite varies considerably with pH and calcium ions concentration. They estimated the dissolution rate with Eq. (8) derived from the general one proposed by Lasaga [66] (Eq. (7)) but omitting the term $f(\Delta G_r)$. For this, they fitted the coefficients k_0 and n_i for hydroxides and calcium ions with the experiments in water and 5.75 mmol/L $Ca(OH)_2$. This led to values of 70 mmol $m^{-2}s^{-1}$ for k_0 and to 0.465 and −0.33 for the exponents of the H^+ and $CaOH^+$ activities respectively. Finally they propose that the C_3S dissolution can be written as:

$$\frac{dC_3S}{dt}\left(\text{mmol}\,s^{-1}\,m^{-2}\right) = 70 \cdot A \cdot (SI-1) \cdot \left[H^+\right]^{0.465}\left[CaOH^+\right]^{-0.33}. \quad (8)$$

The rate of dissolution was measured to be 10.92 μmol $m^{-2}s^{-1}$ in demineralised water and decreased by almost a factor of 5 in a 5.75 mM lime solution and by a factor of 218 for saturated lime conditions. The latter measurement gave a rate of dissolution of 0.05 μmol $m^{-2}s^{-1}$ which is 10 times lower than the value calculated using the above equation (see Table 2). Damidot and co-workers [9] attributed this discrepancy to the precipitation of a surface layer on C_3S.

A problem with this formula is that the rate tends to infinity in very dilute solution because of its dependency on $[CaOH^+]$ to a negative power. Therefore, such a simplification can only work over a limited range of solution compositions. Moreover, this Eq. (8) does not take into account the $f(\Delta G_r)$ factor. This factor relates the velocity of the dissolving steps from a dislocation core as a function of the change in Gibbs free energy and depends on the ΔG^*_{crit} term (for more details see [2]). Nonlinearity in the rate of dissolution should appear around ΔG^*_{crit} which is the barrier for etch pits to open up, and a substantial reduction in the rate of dissolution should be seen, as can indeed be observed in Figs. 6 and 19 [2]. $|\Delta G^*_{crit}|$ values are rather large for minerals (from 2 to several kJ/mol) [2,50]. Neglecting this parameter could easily account for the error of one order of magnitude between the rate calculated at higher calcium hydroxide concentration (22 mmol $Ca(OH)_2$) and the experimental value. Lasaga and Lüttge [2] themselves underline that linear extrapolation of data from regions of high undersaturation to the equilibrium point (i.e., rate = 0 at $\Delta G = 0$) will substantially overestimate the dissolution rates as equilibrium conditions are approached.

Table 2
Average and calculated dissolution rate for pure C_3S in different lime solutions after 0.1 s of dissolution with W/S = 0.5 and SSA = 4265 cm^2g^{-1} [9].

Electrolyte	Water	$Ca(OH)_2$ 5.75 mmol/L	$Ca(OH)_2$ 22 mmol/L
Average rate μmol $m^{-2}s^{-1}$	10.92	2.07	0.05
Average rate μmol $m^{-2}s^{-1}$	10.91	2.01	0.54

5.3. Understanding the effect of portlandite and lime additions

Odler and Dörr [35] observed that the initial addition of portlandite crystals increased the induction period, which led them to conclude that the induction period was not brought to an end by the precipitation of this phase. Brown and co-workers [69] noticed that hydration of pure C_3S in saturated lime solution with a water to binder ratio of 0.6 was retarded compared to hydration with demineralised water. However, in the first case portlandite would dissolve quickly in the initial conditions of undersaturation that follow water addition, increasing the calcium ion concentration and decreasing the undersaturation, so slowing dissolution and prolonging the induction period. In the second case, the use of saturated lime solution slows the dissolution from the start and so prolongs the induction period.

It was also found that an addition of 2.5% of free lime by weight of C_3S prolongs the induction period but that higher amounts shorten it [25]. These phenomena can be interpreted from the dissolution point of view as the fast dissolution of free lime rapidly increases the quantity of calcium ions in solution and lowers the undersaturation with respect to the anhydrous phases. This will prevent fast dissolution of alite and etch pit formation and consequently increase the duration of the induction period. However, at higher additions, the free lime may act as a nucleation site for the precipitation of the hydrates or possibly simply by local heating if the temperature was not very well controlled in these experiments.

6. Proposed mechanisms of early hydration of alite

New experiments and a reassessment of previously published results show that, the saturation state of the solution has a critical influence on the rate of reaction of alite. For alite in contact with deionised water, the undersaturation coefficient is initially very large. All the dissolution mechanisms discussed above are active leading to the fast release of ions into solution and a high rate of heat evolution, but also to a rapid increase in the concentration of ions in solution and so a decrease in undersaturation. During this initial period of high undersaturation etch pits could form on plain surfaces (regime III, Fig. 4), but this period of very large undersaturation will quickly give way to the regime in which etch pits form only at the point of emergence of crystallographic defects with the surface. This corresponds to zone II in Figs. 6 and 20. After a few minutes, as the concentration of ions continues to increase, decreasing therefore the undersaturation below that needed to overcome the activation energy (ΔG_{crit}) for the creation of etch pits; the dissolution slows down as it is limited to step retreat at pre-existing steps. This transition from fast to slow dissolution is symbolized by the arrow 1 in Fig. 20. This process corresponds to the onset of the period of low chemical activity, the "induction period". Thus dissolution theory can explain the onset of the induction period without having to invoke additional mechanisms such as the formation of a protective membrane.

It is interesting to note that the transition to slow dissolution occurs at concentrations around those of saturated calcium hydroxide, as shown schematically in Fig. 20. For this reason it is not possible to verify the existence of the plateau of slow dissolution as more concentrated solutions will precipitate calcium hydroxide and lower the concentration. In the regime undersaturated with respect to calcium hydroxide, the rate of dissolution varies smoothly as found experimentally by Damidot et al. [9] (Fig. 20). During the induction period, the solution is progressively enriched in calcium and

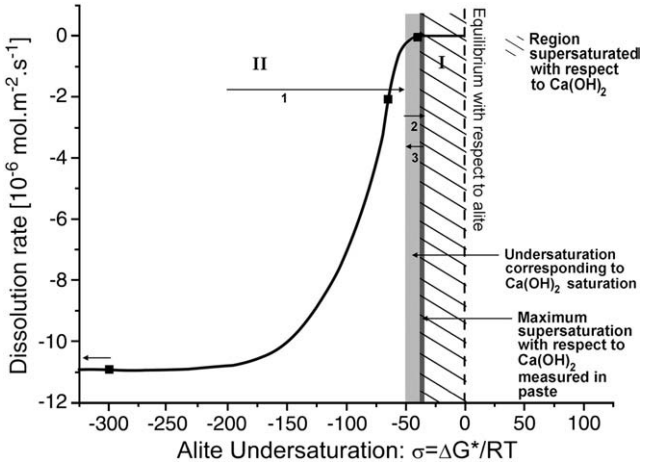

Fig. 20. Schematic representation of the rate of dissolution of alite as a function of the undersaturation. The black squares represent the experimental data obtained by Damidot and co-workers (see Table 2) [9] and the plain curve is the assumed evolution of the rate of dissolution of alite as a function of the undersaturation. The light grey zone correspond to portlandite saturation which is assumed to be close to $\Delta G_{crit}^{*}/RT$ (the width correspond to the uncertainty in silicate ions concentration). This value delimits the fast dissolution regime controlled by etch pit formation (zone II) and the slow regime of dissolution where only step retreat takes place (zone I). Arrows 1, 2 and 3 show the evolution of the undersaturation during respectively the fast dissolution stage, the induction or "dormant" period and finally the acceleration period (see also Fig. 1).

hydroxides, causing the system to approach the critical supersaturation of portlandite (arrow 2 in Fig. 20).

As the solution quickly becomes saturated with respect to C–S–H, precipitation of this hydrate may occur, but this is not responsible for the onset of the induction period (strong reduction in rate of heat release). To support this argument, it can be noted that, as observed in the studies presented here (Fig. 7) and also reported by Zingg and co-workers [44], these primary hydrates do not form any visible continuous layer around the anhydrous grains.

At the end of the induction period the growth of hydrates lowers the concentration of ions in solution (increase the undersaturation). This increases alite undersaturation and brings the system back towards undersaturations where alite dissolution may take place in mode II (arrow 3 in Fig. 20). However, at this stage it is most probably the hydrate growth becomes rate controlling. Results of C–S–H seeding experiments done by Thomas and co-workers [70] supports this view as it shows that the induction period could be suppressed by the addition of 4% by weight of cement of C–S–H seeds. It seems however that the C–S–H seeds have to be different from primary C–S–H hydrates in order to enable the instantaneous onset of the acceleration period.

It appears that the induction period ends when a critical amount of dissolution (and consequently product formation) has occurred as a lower heat output during the induction period corresponds to a longer induction period as seen in our experiments on the annealing of alite, and in studies by Costoya [52] of alites with different particle sizes. However, the exact process which brings the induction period to an end is still unclear. At present the most reasonable explanation is that C–S–H (possibly of a different structure to that formed initially) starts to grow in a rapid manner (which could be due to enough surface having been created or the presence of particular reactive sites in the C–S–H enabling a faster growth) consuming rapidly the ions in solution and therefore controlling the rate of dissolution of alite. Fig. 21 presents schematically the hydration process at very early ages at a microscopic level.

In regard to the above proposed mechanism of alite hydration, it is clear that any change of the critical undersaturation with respect to alite, or of the critical supersaturation with respect to portlandite, can be expected to have a profound impact on alite hydration kinetics. The implications of these findings in terms of working mechanisms of accelerators and retarders remain however to be studied.

7. Conclusions

There are two outstanding questions regarding the early hydration of C_3S and alite. The first concerns the very fast deceleration of reactivity that follows the burst in reactivity after contact with water. The second concerns the onset of the acceleration period that follows a period of low chemical reactivity.

In this paper we show how the dissolution theory developed in the field of geochemistry can explain the initial slowdown in reaction without the need to suppose the formation of a protective phase. When the level of undersaturation drops below that needed to provide enough energy for the nucleation of etch pits at dislocations,

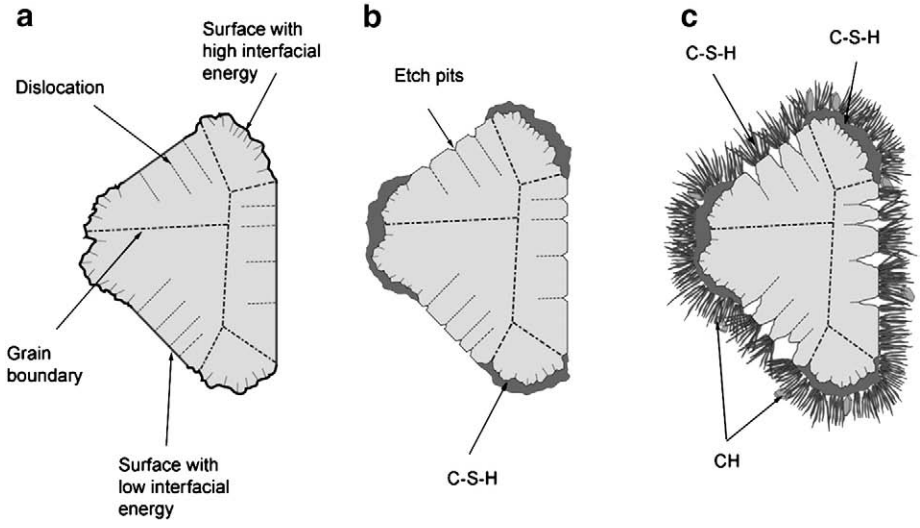

Fig. 21. Hydration scheme at early age of reaction. (a) An alite grain is represented in cross section. Dislocations and grain boundaries are represented by solid and dashed lines. (b) When the alite grain is put in contact with water, we assume that some primary hydrates will precipitate (C–S–H in dark gray) but not as a continuous membrane. Areas of lower surface energy might remain only partially hydroxylated and will therefore present some etch pitting at the point of emergence of dislocations. Note that dislocations do not end up in grains but here we assume that other dislocations may cross them leading the represented dislocations to slip on other crystallographic planes. (c) Finally stable nuclei of CH and C–S–H start to grow. This marks the end of the induction period and the beginning of the acceleration period.

the rate of dissolution becomes slow as atoms may dissolve only from preformed steps.

We provide evidence for this mechanism in the form of new experimental observations and a re-examination of results in the literature, which show:

- A very strong dependence of the rate of dissolution on the concentration of the solution.
- The formation of numerous etch pits on alite surface mixed with deionised water, in contrast to a dominance of smooth surfaces with formation of steps in the case of lime saturated solutions.
- A strong influence of defect density on the rate of dissolution during the induction period and therefore its length and the variation in density of etch pits as a function of crystallographic orientation.

Experimental data from other minerals exhibits a nonlinear step change in dissolution rate at levels of undersaturation significantly larger than expected from transition state theory. Comparison of the typical energy barriers for etch pit formation from such minerals to the case of alite indicates that the large difference in concentration between typical hydrating pastes and the equilibrium solubility of alite falls within the magnitude expected for a dissolution limited by the formation of etch pits. Such energy barriers also explain inconsistencies in dissolution rates extrapolated from very high levels of undersaturation.

The mechanism responsible for the onset of the acceleration period remains open, but this appears to occur after a critical amount of dissolution. The onset of rapid growth of C–S–H (which could just be due to the development of a sufficiently large C–S–H surface or due to the development of specific reactive sites in C–S–H) appears to be the most likely cause for the onset of the acceleration period. The time to reach this event is affected by the change of dissolution rate discussed in this paper.

Acknowledgements

The authors would like to acknowledge the help of Dr. M. Costoya for assistance in certain experiments and also Sika Technology AG for financial support. In addition, we would like to thank Dr. B. Lindlar and Dr. D. Lootens for constructive discussions.

References

[1] P.M. Dove, N. Han, J.J. De Yoreo, Mechanisms of classical crystal growth theory explain quartz and silicate dissolution behaviour, PNAS 102 (43) (2005) 15357–15362.
[2] A.C. Lasaga, A. Lüttge, Variation of crystal dissolution rate based on a dissolution stepwave model, Science 291 (2001) 2400–2404.
[3] K. Sangwal, Etching of Crystals, vol. 15, North-Holland, 1987.
[4] P.C. Lichtner, Continuum model for simultaneous chemical reactions and mass transport in hydrothermal systems, Geochimica et Cosmochimica Acta 49 (3) (1985) 779–800.
[5] P.C. Lichtner, The quasi-stationary state approximation to coupled mass transport and fluid rock interaction in a porous medium, Geochimica et Cosmochimica Acta 52 (1) (1988) 143–165.
[6] P. Barret, D. Ménétrier, Filter dissolution of C_3S as a function of lime concentration in a limited amount of lime water, Cement and Concrete Research 10 (1980) 521–534.
[7] P. Barret, D. Ménétrier, D. Bertrandie, Mechanism of C_3S dissolution and the problem of congruency in the very initial period and later, Cement and Concrete Research 13 (1983) 728–738.
[8] L. Nicoleau. Interactions physico-chimiques entre latex et les phases minérales constituant le ciment au cours de l'hydratation, Ph. D. Thesis (2004).
[9] D. Damidot, F. Bellman, B. Möser, T. Sowoidnich, Modelling the effect of electrolytes on the rate of early hydration of tricalcium silicate, in: W. Sun, K. van Breugel, C. Miao, G. Ye, H. Chen (Eds.), 1st International Conference on Microstructure Related Durability of Cementitious Composites, RILEM Proceedings PRO, vol. 61, China, Nanjing, 2008, pp. 1075–1081.
[10] J.B. Johnson, S.J. Haneef, B.J. Hepburn, A.J. Hutchinson, G.E. Thompson, G.C. Wood, Laboratory exposure systems to simulate atmospheric degradation of building stone under dry and wet deposition conditions, Atmospheric Environment Part A, General Topics 24A (10) (1990) 2585–2592.
[11] A. Moropoulou, K. Bisbikou, K. Torfs, R. van Grieken, F. Zezza, F. Macri, Origin and growth of weathering crusts on ancient marbles in industrial atmosphere, Atmospheric Environment 32 (1998) 967–982.
[12] H. Okochi, H. Kameda, S. Hasegawa, N. Saito, K. Kubota, M. Igawa, Deterioration of concrete structures by acid deposition — an assessment of the role of rainwater on deterioration by laboratory and field exposure experiments using mortar specimens, Atmospheric Environment 34 (2000) 2937–2945.
[13] S.V. Dorozhkin, Dissolution models of calcium apatites, Progress in Crystal Growth and Characterization of Materials (2002) 45–61.
[14] M.L.D. Gougar, B.E. Scheetz, D.M. Roy, Ettringite and C–S–H Portland cement phases for waste ion immobilization: a review, Waste Management 16 (4) (1996) 295–303.
[15] E.M. Gartner, J.F. Young, D.A. Damidot, I. Jawed, Structure and Performance of Cements, 2nd editionSpon Press, 2002.
[16] H.F.W. Taylor, Cement Chemistry, 2nd ed.Thomas Telford Publishing, 1997.
[17] I. Odler, Lea's Chemistry of Cement and Concrete, Arnold, 1998.
[18] J.P. Skalny, J.F. Young, Mechanisms of Portland Cement Hydration, *7th ISCC*, 1980, 1, II-1/3-II-1/45.
[19] Le. Châtelier, Recherches expérimentales sur la constitution des mortiers hydrauliques, Dunod, 1904.
[20] H.N. Stein, J.M. Stevels, Influence of silica on the hydration of 3CaO, SiO_2, Journal of Applied Chemistry 14 (1964) 338–346.
[21] D.L. Kantro, S. Brunauer, C.H. Weise, Development of surface in the hydration of calcium silicates. II. Extension of investigations to earlier and later stages of hydration, Journal of Chemical Chemistry 66 (10) (1962) 1804–1809.
[22] E.M. Gartner, H.M. Jennings, Thermodynamics of calcium silicate hydrates and their solutions, Journal of the American Ceramic Society 70 (10) (1987) 743–749.
[23] E.M. Gartner, J.M. Gaidis, Hydration mechanisms, I, in: J.P. Skalny (Ed.), The Materials Science of Concrete, I, American Ceramic Society, 1989, pp. 95–125.
[24] P.W. Brown, E. Franz, G. Frohnsdorff, H.F.W. Taylor, Analyses of the aqueous phase during early C_3S hydration, Cement and Concrete Research 14 (1984) 257–262.
[25] J.G.M. de Jong, H.N. Stein, J.M. Stevels, Hydration of tricalcium silicate, Journal of Applied Chemistry 17 (1967) 246–250.
[26] R. Kondo, M. Daimon, Early hydration of tricalcium silicate: a solid reaction with induction and acceleration period, Journal of the American Ceramic Society 52 (9) (1969) 503–508.
[27] H.M. Jennings, P.L. Pratt, An experimental argument for the existence of a protective membrane surrounding Portland cement during the induction period, Cement and Concrete Research 9 (1979) 501–506.
[28] J.D. Birchall, A.J. Howard, J.E. Bailey, On the hydration of Portland cement, Proceedings of the Royal Society A 360 (1978) 445–453.
[29] D.D. Double, A. Hellawell, S.J. Perry, The hydration of Portland cement, Proceedings of the Royal Society A 359 (1979) 435–451.
[30] M.E. Tadros, J. Skalny, R.S. Kalyoncu, Early hydration of tricalcium silicate, Journal of the American Ceramic Society 59 (7–8) (1976) 344–347.
[31] I. Odler, J. Schüppstuhl, Early hydration of tricalcium silicate III. Control of the induction period, Cement and Concrete Research 11 (1981) 765–774.
[32] T. Sakurai, T. Sato, A. Yoshinaga, The effect of minor components on the early hydraulic activity of the major phases of Portland cement clinker, 5th ISCC 1, 1969, pp. 300–321.
[33] J.N. Maycock, J. Skalny, R. Kalyoncu, Crystal defects and hydration I. Influence of lattice defects, Cement and Concrete Research 4 (1974) 835–847.
[34] P. Fierens, J.P. Verhaegen, Hydration of tricalcium silicate in paste — kinetics of calcium ions dissolution in the aqueous phase, Cement and Concrete Research 6 (1976) 337–342.
[35] I. Odler, H. Dörr, Early hydration of tricalcium silicate II. The induction period, Cement and Concrete Research 9 (1979) 277–284.
[36] S. Garrault, A. Nonat, Experimental investigation of calcium silicate hydrate (C–S–H) nucleation, Journal of Crystal Growth 200 (1999) 565–574.
[37] S.A. Rodgers, G.W. Groves, N.J. Clayden, C.M. Dobson, Hydration of tricalcium silicate followed by ^{29}Si NMR with cross-polarization, Journal of the American Ceramic Society 71 (2) (1988) 91–96.
[38] O.S. Pokorovsky, S.V. Golubev, J.A. Mielczarski, Kinetic evidences of the existence of positively charged species at the quartz-aqueous solution interface, Journal of Colloid and Interface Science 296 (2006) 189–194.
[39] S.C. Parker, J.P. Allen, C. Arrouvel, D. Spagnoli, S. Kerisit, D.C. Sayle, Molecular simulation of mineral surfaces and the role of impurities on surface stabilities, AIP Conference Proceedings 916 (2007) 268–287.
[40] D. Spagnoli, D.J. Cooke, S. Kerisit, S.C. Parker, Molecular dynamics simulations of the interaction between the surfaces of polar solids and aqueous solutions, Journal of Materials Chemistry 16 (2006) 1997–2006.
[41] J.F. Young, H.S. Tong, R.L. Berger, Compositions of solutions in contact with hydrating tricalcium silicate pastes, Journal of the American Ceramic Society 60 (5–6) (1977) 193–198.
[42] D. Damidot, A. Nonat, C_3S hydration in diluted and stirred suspensions: (I) study of the two kinetic steps, Advances in Cement Research 6 (21) (1994) 27–35.
[43] S. Garrault, E. Finot, E. Lesniewska, A. Nonat, Study of C–S–H growth on C_3S surface during its early hydration, Materials and Structures 38 (2005) 435–442.
[44] A. Zingg, F. Winnefeld, L. Holzer, J. Pakusch, S. Becker, L. Gauckler, Adsorption of polyelectrolytes and its influence on the rheology, zeta potential and microstructure of various cement and hydrate phases, Journal of Colloid and Interface Science 323 (2008) 301–312.
[45] D. Ménétrier, I. Jawed, T.S. Sun, J. Skalny, ESCA and SEM studies on early C_3S hydration, Cement and Concrete Research 9 (1979) 473–482.
[46] P.M. Dove, N. Han, Kinetics of mineral dissolution and growth as reciprocal microscopic surface processes across chemical driving force, AIP Conference Proceedings 916 (2007) 215–234.

[47] A.J. Malkin, Y.G. Kuznetsov, A. McPherson, In situ atomic force microscopy studies of surface morphology growth kinetics, defect structure and dissolution in macromolecular crystallization, Journal of Crystal Growth 196 (1999) 471–488.
[48] N. Cabrera, M.M. Levine, On the dislocation theory of evaporation of crystals, Philosophical Magazine 1 (5) (1956) 450–458.
[49] H.H. Teng, Controls by saturation state on etch pit formation during calcite dissolution, Geochimica et Cosmochimica Acta 68 (2004) 253–262.
[50] T.E. Burch, K.L. Nagy, A.C. Lasaga, Free energy dependence of albite dissolution kinetics at 80 °C and pH 8.8, Chemical Geology 105 (1993) 137–162.
[51] A.C. Lasaga, A.E. Blum, Surface chemistry, etch its and mineral water reactions, Geochimica et Cosmochimica Acta 50 (1986) 2363–2379.
[52] M.M. Costoya. Effect of particle size distribution on the hydration kinetics and microstructural development of tricalcium silicate, Ph. D. Thesis, (2008).
[53] R.B. Williamson, Constitutional supersaturation in Portland cement solidified by hydration, Journal of Crystal Growth 3 (4) (1968) 787–794.
[54] M.C.G. Juenger, P.J.M. Monteiro, E.M. Gartner, G.P. Denbaux, A soft X-ray microscope investigation into the effects of calcium chloride on tricalcium silicate hydration, Cement and Concrete Research 35 (2005) 19–25.
[55] D. Damidot, A. Nonat, C_3S hydration in diluted and stirred suspension: (II) properties of C–S–H precipitated during the two kinetic steps, Advances in Cement Research 6 (22) (1994) 83–91.
[56] S. Garrault, A. Nonat, Hydrated layer formation on tricalcium and dicalcium silicate surfaces: experimental study and numerical simulations, Langmuir 17 (2001) 8131–8138.
[57] P. Fierens, J. Tirlocq, J.P. Verhaegen, Luminescence et hydratation du silicate tricalcique, Cement and Concrete Research 3 (1973) 549–560.
[58] P. Fierens, J. Tirlocq, J.P. Verhaegen, Défauts de structure et hydratation du silicate tricalcique, Industrie Chimique Belge 39 (1974) 363–367.
[59] P. Fierens, J. Tirlocq, J.P. Verhaegen, Influence du mode d'excitation sur la thermoluminescence du silicate tricalcique, Cement and Concrete Research 3 (1973) 227–232.
[60] K.E. Hudson, G.W. Groves, The structure of alite in Portland cement clinker — TEM evidence, Cement and Concrete Research 12 (1982) 61–68.
[61] R.T. Cygan, W.H. Casey, M.B. Boslough, H.R. Westrich, M.J. Carr, G.R. Holdren, Dissolution kinetics of experimentally shocked silicate minerals, Chemical Geology 78 (1989) 229–244.
[62] J.M. Makar, G.W. Chan, End of induction period in ordinary Portland cement as examined by high-resolution scanning electron microscopy, Journal of the American Ceramic Society 91 (4) (2008) 1292–1299.
[63] H. di Murro Mécanismes d'élaboration de la microstructure des bétons, Ph. D. Thesis (2007).
[64] H.N. Stein, Thermodynamic considerations on the hydration mechanisms of Ca_3SiO_5 and $Ca_3Al_2O_6$, Cement and Concrete Research 2 (1972) 167–177.
[65] K. Mishra, H. Heinz, Atomistic Simulation of Cleavage Energy of C_3S and Organic-silicate Interactions in *Challenges and promises of multi-scale modelling schemes for cementitious materials workshop*, Derio (Spain), 2–4 mars, 2009.
[66] A.C. Lasaga, Kinetic Theory in the Earth Sciences, Princeton University Press, 1998.
[67] J.W. Bullard, A determination of hydration mechanisms for tricalcium silicate using a kinetic cellular automaton model, Journal of the American Ceramic Society 91 (7) (2008) 2088–2097.
[68] J.W. Bullard, Presentation: "Three-Dimensional Structural Modelling of Cement Hydration: Opportunities for Bridging Length Scales", *Challenges and promises of multi-scale modelling schemes for cementitious materials workshop*, Derio (Spain), 2–4 mars, 2009.
[69] P.W. Brown, C.L. Harner, E.J. Prosen, The effect of inorganic salts on tricalcium silicate hydration, Cement and Concrete Research 16 (1985) 17–22.
[70] J.J. Thomas, H.M. Jennings, J.J. Chen, Influence of nucleation seeding on the hydration mechanisms of tricalcium silicate and cement, Journal of Physical Chemistry C 113 (2009) 4327–4334.